A unified algorithm for moving interfaces and mixing zones in a multi-component compressible fluid model

Bruno Després [a,b] Frédéric Lagoutière [a]

[a] *Laboratoire J.-L.-Lions, Université P.-et-M.-Curie, 175, rue du Chevaleret, 75013 Paris, France*

[b] *Commissariat à l'Énergie Atomique, BP12, 91680 Bruyères-le-Châtel, France*

Abstract

We study a unified algorithm for moving interfaces and mixing zones in a multi-component compressible fluid. We propose to use the downwind limited scheme (also called Ultra-Bee limiter in the context of pure advection), in order to avoid any artificial numerical spreading of interfaces or mixing zones. Various numerical simulations show the interest of this approach, for both interfaces and static/dynamic mixing zones.

Key words: Finite volume, interfaces, static mixing zones, dynamic mixing zones, anti-dissipative algorithm.

1 Introduction

We address a unified algorithm for handling interfaces and mixing zones in a multi-component compressible fluid. Let us take a simple idealized example in order to describe what we are interested in. We consider a two-fluid compressible problem and make the hypothesis that these two fluids may be considered as separated by an interface at $t = 0$. Then we let the system move freely due to some velocity or pressure gradients. At this point two situations with very different physical meanings at the macroscopic level may occur.

case a) Interfaces The first case is that interfaces still exist at the macroscopic level for any time $T > 0$. The length of the interface may be a dramatically increasing function of time, as it is the case in figure 1. Nevertheless we assume an interface is still a good modeling.

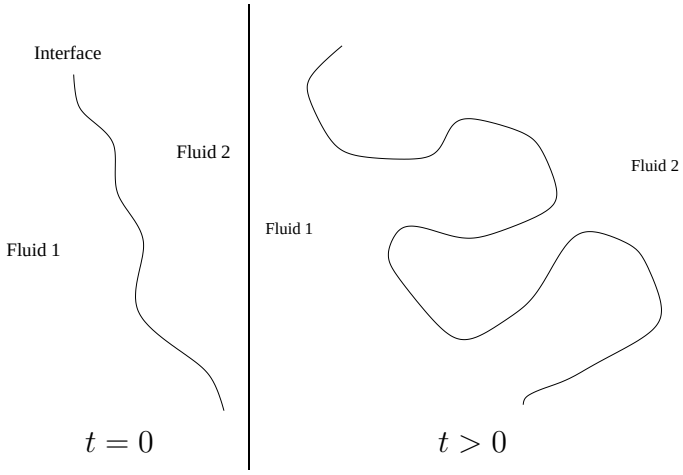

Fig. 1. Interface

In this case an interface tracking or interface reconstruction algorithm is enough for the numerical simulation, even if it is well-known that such algorithms are sometimes very delicate to couple with fluid models.

case b) Interfaces and mixing zones The second case is that some mixing process tends to replace the initial interface with a mixing zone, so interfaces disappear and are replaced by mixing zones at the macroscopic level (see [11], [14] for a presentation).

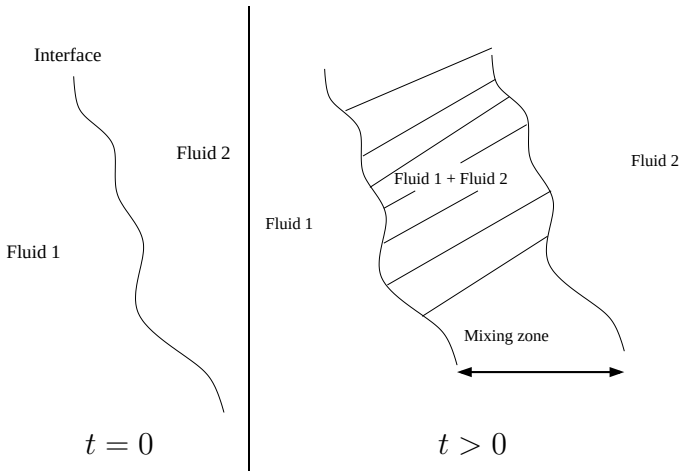

Fig. 2. Transition interface-mixing zone

The microscopic mechanism responsible for the transition interface-mixing zone may be a molecular diffusion process, turbulence and/or the final stage of hydrodynamic instabilities. Of course this is highly dependent on the physical situation under study. At the numerical level, an interface tracking or interface reconstruction algorithm is not enough: another algorithm is needed in order the numerical modeling of the mixing zone to be correct. The study

of the transition between interfaces and mixing zones is our main motivation for the design of numerical algorithms with the ability to take into account both interfaces and mixing zones. In this work we focus more on the numerical algorithm, and not on the set of partial differential equations that one needs to model the transition. In other terms, we consider more a **static transition** than a **dynamic transition**. However we study in section 6 a very simple and naive dynamic model in order to demonstrate that our algorithm is able to take into account some **dynamic transition**. Among many algorithms for interface tracking, interface reconstruction or pseudo-interface reconstruction, let us refer to [10] for interface tracking, [26] for VoF type methods, [9] for the Ghost Fluids Method, and [20] for the SLIC algorithm, which is the first algorithm published for this kind of problems. In the case of a multi-component fluid problem with interfaces, the validity of these algorithms has been demonstrated since a long time: a recent review about VoF methods is [3] (Colella 2001); see also references therein. Even if VoF type methods have many advantages particularly for the discretization stage, some researchers feel the need for a more PDE-based formulation of these interface multi-component fluid problems: an example is the Level Set method [21]. All these algorithms are useful for the situation described in **case a)**. An alternative to interface tracking or interface reconstruction is to follow some concentration equations for the components of the fluid. For example

$$\partial_t(\rho c) + \mathrm{div}(\rho c \vec{u}) = 0, \tag{1}$$

where c is a mass fraction, volume fraction or color function. If $c = 0$ or $c = 1$ at $t = 0$ (it means that an interface separates the two fluids at $t = 0$), then it is enough to discretize the concentration equation (1) (cf. [8] for example). This approach has many advantages for mixing zones: see [1], [2]. However the well-known drawback of that approach is that standard Finite Volume numerical schemes are dissipative for discontinuous initial profiles.

The main idea of this work is to use (1) in conjunction with an interesting property of the downwind limited scheme (also called the Ultra-Bee scheme when applied to linear advection, cf. [25]) see [7], [18], [6]. In [6] it is proved that the downwind limited scheme is, in 1D, in some sense exact for the transport of discontinuous data. We show that a x-y splitting strategy on Cartesian grid with the limited downwind scheme is a solution for a unified numerical treatment of **case a)** and **case b)** in the context of a multi-component compressible fluid. The algorithm is very much in the spirit of VoF method when applied to multi-material flows with interfaces ([3], [17]), except for the transport algorithm which is probably simpler than many other algorithms. It is clearly this unique feature of the transport algorithm used in this work that allows to construct a unified algorithm for multi-material flows with interfaces and mixing zone. The essential mathematical properties of the proposed algorithm may be resumed in the following results, that guarantees the non-dissipation

of interfaces and the stability of the algorithm.

Result 1 exact transport of some discontinuous profiles The limited downwind scheme (17) allows to compute exact solutions of advection equation for initial conditions that are step functions, provided that the cells are small enough: at least 3 cells per step of the initial condition (see theorem 1).

Result 2 entropy inequalities Under a CFL-like condition, the scheme verifies entropy properties: the numerical value of the physical entropy of each component increases locally. In particular one has

$$S_{r_j}^{n+1} \geq \min_j(S_{r_j}^n) \quad r = 1, 2 \text{ and } \forall j, n,$$

where $S_{r_j}^n$ denotes the entropy of fluid $r = 1, 2$ in the cell j at time step n (see propositions 1 and 2).

A plan of this work follows. In section 2 we present a family of models that serves for the modeling in our two-component compressible fluid simulations. Section 3 is devoted to the presentation of the main features of the downwind limited scheme. In section 4 we generalize the downwind limited scheme to the two-components fluid models and give some of its mathematical properties. In section 5 we present various numerical simulations in order to give an overview of the capabilities of the algorithm; we give in section 6 a simple example with dynamic mixing.

2 A family of models

For the sake of simplicity the presentation is restricted to a two-fluid model (see [18] for the general case). ρ is the density of the global fluid, ρc_1 (resp. ρc_2) is the partial density of fluid number one (resp. number two). It means that $c_1 + c_2 = 1$. The velocity of the global fluid is denoted as $\vec{u}$. We make the assumption that the velocities of both fluids are equal, that is

$$\vec{u_1} = \vec{u_2} = \vec{u}. \tag{2}$$

The total energy is denoted as e:

$$e = c_1\varepsilon_1 + c_2\varepsilon_2 + \frac{1}{2}|\vec{u}|^2 \tag{3}$$

where ε_1 and ε_2 are the internal energies of each fluid. The total pressure will be denoted as p. Next we describe an important property of the family of models considered in this work. We consider that there exists a scale at which the two fluids are separated. In other words it means that the pressure

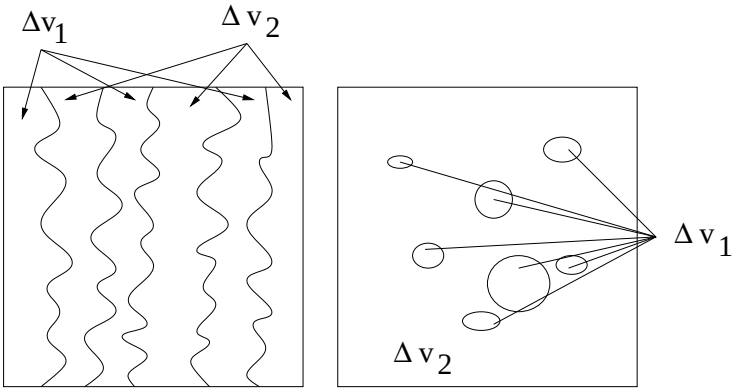

Fig. 3. All microscopic structures of the mixture are admissible.

is not a function of the apparent densities $\rho_1 = \rho c_1$ and $\rho_2 = \rho c_2$, but is a function of the (true) densities: this consideration is based on the notion of additivity of volumes. We assume that any elementary volume Δv is the sum of two sub-volumes Δv_1 and Δv_2, $\Delta v = \Delta v_1 + \Delta v_2$, and that only the first (resp. second) fluid is present in Δv_1 (resp. Δv_2). Here we do not make any hypothesis on the shape of these Δv_1 and Δv_2, as in figure 3. The total mass in Δv is $\Delta m = \rho \Delta v$. Mass fractions c_1, c_2 and partial masses Δm_1 and Δm_2 are related through $c_1 = \frac{\Delta m_1}{\Delta m}$ and $c_2 = \frac{\Delta m_2}{\Delta m}$. Since $\Delta m_1 + \Delta m_2 = \Delta m$, one has $c_1 + c_2 = 1$. The true density of fluid number 1 (resp. 2) is denoted as $\overline{\rho}_1$ (resp. $\overline{\rho}_2$). It means that $\Delta m_1 = \overline{\rho}_1 \Delta v_1 = c_1 \rho \Delta v$ and $\Delta m_2 = \overline{\rho}_2 \Delta v_2 = c_2 \rho \Delta v$. We deduce that $\frac{1}{\rho}(\Delta v_1 + \Delta v_2) = (\frac{c_1}{\overline{\rho}_1} + \frac{c_2}{\overline{\rho}_2})\Delta v$. Thus the additivity of volumes is equivalent to $\frac{1}{\rho} = \frac{c_1}{\overline{\rho}_1} + \frac{c_2}{\overline{\rho}_2}$. Defining the specific volume of each fluid $\tau_{1,2} = \frac{1}{\overline{\rho}_{1,2}}$ this equation is

$$\tau = c_1 \tau_1 + c_2 \tau_2, \tag{4}$$

which is the mathematical expression of the additivity of volumes. We propose to compute the pressure in fluid 1 and the pressure in fluid 2 using some Equations of States (EOS), as in

$$p_1 = p_1(\tau_1, \varepsilon_1) \text{ and } p_2 = p_2(\tau_2, \varepsilon_2). \tag{5}$$

For example one may consider situations where a perfect gas approximation is good: $p_1 = (\gamma_1 - 1)\frac{\varepsilon_1}{\tau_1}$, $p_2 = (\gamma_2 - 1)\frac{\varepsilon_2}{\tau_2}$. For the sake of simplicity, we consider only this case in the rest of the work. It remains to describe a mixing model in order to close the model. For example one may choose the isobar-isothermal closure

$$p_1 = p_2, \;\; T_1 = T_2 \tag{6}$$

where $C_{v1} T_1 = \varepsilon_1$ and $C_{v2} T_2 = \varepsilon_2$ for some constants $C_{v1} > 0$ and $C_{v2} > 0$. However we will also consider the "isobar-isoδQ" model

$$p_1 = p_2, \;\; \delta Q_1 = \delta Q_2, \tag{7}$$

where, from the fundamental law of thermodynamic, we have $\delta Q_1 = T_1 dS_1 = d\varepsilon_1 + p_1 d\tau_1$ and $\delta Q_2 = T_2 dS_2 = d\varepsilon_2 + p_2 d\tau_2$. So it is possible to replace $\delta Q_1 = \delta Q_2$ by the incremental partial differential equation

$$\mathrm{D}_t\varepsilon_1 + p_1\mathrm{D}_t\tau_1 = \mathrm{D}_t\varepsilon_2 + p_2\mathrm{D}_t\tau_2, \tag{8}$$

where D_t denotes material derivative: $\mathrm{D}_t = \partial_t + u\partial_x + v\partial_y$ in dimension 2, with $\vec{u} = (u, v)^T$. We here will discuss these two models. They are

$$\begin{cases} \partial_t\rho + \partial_x(\rho u) + \partial_y(\rho v) = 0, \\ \partial_t(\rho c_1) + \partial_x(\rho u c_1) + \partial_y(\rho v c_1) = 0, \\ \partial_t(\rho c_2) + \partial_x(\rho u c_2) + \partial_y(\rho v c_2) = 0, \\ \partial_t(\rho u) + \partial_x(\rho u^2 + p) + \partial_y(\rho uv) = 0, \\ \partial_t(\rho v) + \partial_x(\rho uv) + \partial_y(\rho v^2 + p) = 0, \\ \partial_t(\rho e) + \partial_x(\rho ue + pu) + \partial_y(\rho ve + pv) = 0, \\ p_1 = p_2 = p, \\ \textbf{isothermal } T_1 = T_2 \text{ or } \textbf{iso-}\delta Q \ \mathrm{D}_t\varepsilon_1 + p_1\mathrm{D}_t\tau_1 = \mathrm{D}_t\varepsilon_2 + p_2\mathrm{D}_t\tau_2. \end{cases} \tag{9}$$

These two systems are very similar, except for the mixture model. The isothermal model has the advantage to be fully conservative, while the non conservative iso-δQ model has the advantage to be independent of the determination of C_{v_1} and C_{v_2} because it does not involve the temperature. The second model in (9) is equivalent to the non-conservative partial differential equation

$$\begin{cases} \partial_t\varepsilon_1 + u\partial_x\varepsilon_1 + v\partial_y\varepsilon_1 + p(\partial_t\tau_1 + u\partial_x\tau_1 + v\partial_y\tau_1) \\ = \partial_t\varepsilon_2 + u\partial_x\varepsilon_2 + v\partial_y\varepsilon_2 + p(\partial_t\tau_2 + u\partial_x\tau_2 + v\partial_y\tau_2). \end{cases} \tag{10}$$

When interfaces exist between fluid number one and fluid number two, then one has to understand that (9) is in some sense degenerated. It simply means that c_1 (resp. c_2) takes values only in $\{0, 1\}$: thus $c_1 c_2 = 0$ everywhere. In this case the isobar relation is only here for the treatment of mixed cells in the numerical stage. The numerical treatment of the interface-configuration (at the continuous level) is responsible for the numerical mixing-configuration. In figure 4 we give an example. Nevertheless (9) will also be used in the case of a true mixing zone.

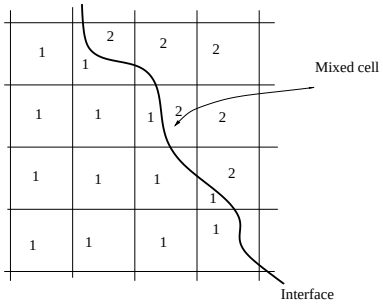

Fig. 4. Interface and mixed cells

3 The basic scheme for moving interfaces and mixing zones

Let us consider a situation where the velocity is constant $(u, v) = \text{constant}$, and the pressure is constant $p_1 = p_2 = \text{constant}$. In this case (9) reduces to pure transport. It means that our algorithm has to degenerate to the numerical solution of $\partial_t c + u\partial_x c + v\partial_y c = 0$ in 2D, or $\partial_t c + u\partial_x c = 0$ in 1D. The difficulty is that we require that the transport algorithm is able to transport both Heavyside initial profiles **and** smooth initial profiles. We assume that the transport algorithm may be rewritten in the Finite Volume setting

$$\frac{c_j^{n+1} - c_j^n}{\Delta t} + u\frac{c_{j+\frac{1}{2}}^n - c_{j-\frac{1}{2}}^n}{\Delta x} = 0, \quad u > 0. \tag{11}$$

The new value of the unknown is c_j^{n+1}. It is a function of (c_j^n) and of the fluxes $(c_{j+\frac{1}{2}}^n)$. Let us describe the main ingredient of our basic transport scheme. First let us look at the very simple situation where the initial solution c^0 is a Heavyside function: this is the prototype of an interface.

$$c_l^0 = 1, \quad \forall l \leq j, \text{ and } c_l^0 = 0, \quad \forall l > j. \tag{12}$$

Let us assume that the time step is not the maximal time step. For example $u\frac{\Delta t}{\Delta x} = \frac{1}{3} < 1$. For the initial condition (12), the exact solution at the first time step is $c^0(x - \frac{\Delta x}{3})$. After projection on the grid, it is $c_l^1 = \frac{1}{\Delta x}\int_{x_{l-\frac{1}{2}}}^{x_{l+\frac{1}{2}}} c^0(x - \frac{\Delta x}{3})dx$, that is,

$$c_l^1 = 1 \quad l \leq j, \quad c_{j+1}^1 = \frac{1}{3}, \quad c_l^1 = 0 \quad l > j+1. \tag{13}$$

At the second time step, the exact solution is $c^0(x - \frac{2\Delta x}{3})$ while the projected exact solution is $c_l^2 = \frac{1}{\Delta x}\int_{x_{l-\frac{1}{2}}}^{x_{l+\frac{1}{2}}} c^0(x - \frac{2\Delta x}{3})dx$ that is

$$c_l^2 = 1 \quad \forall l \leq j, \quad c_{j+1}^2 = \frac{2}{3}, \quad c_l^2 = 0 \quad \forall l > j+1. \tag{14}$$

After a third time step, the exact solution is $c^0(x-\Delta x)$. Its projection on the grid is

$$c_l^3 = 1, \quad \forall l \leq j+1, \text{ and } c_l^3 = 0, \quad \forall l > j+1, \tag{15}$$

and is again equal to the exact solution 4. Now we forget that (12), (13), (14) and (15) are some cell-averages of the exact solution, and consider that these numerical profiles are given by a finite volume scheme (11). If we try to define some numerical fluxes such that the scheme (11) applied to the initial condition (12) (resp. (13) or (14)) gives (13) (resp. (14) or (15)), a solution for the cell j is $c_{j-\frac{1}{2}}^{1,2} = 1$ and $c_{j+\frac{1}{2}}^{1,2} = 0$. Indeed it implies $c_{j+\frac{1}{2}}^1 = 0$, $c_j^1 = \frac{1}{3}$, $c_{j+1}^1 = 0$. So we arrive at the conclusion that in this situation the "exact numerical flux", between cell j and cell $j+1$, is equal to the down-winded value of the exact solution, that is $c_{j+\frac{1}{2}}^{1,2} = c_{j+1}^{1,2}$. Now we raise this simple fact is a general principle for the choice of the numerical flux. The numerical flux will be chosen as closed as possible to the **down-winded** value of the numerical solution. However it is well-known that the downwind linear scheme (i.e. $c_{j+\frac{1}{2}} = c_{j+1}$) is unstable. So we need to incorporate some stability and TVD (stands for Total Variation Diminishing) notions in order to get a stable and convergent scheme. What we emphasize on is that it is possible to add some TVD constraints in the choice $c_{j+\frac{1}{2}} = c_{j+1}$ such that: if possible we take $c_{j+\frac{1}{2}} = c_{j+1}$; otherwise we take $c_{j+\frac{1}{2}}$ to be the closest as possible value to c_j. Following the approach presented in detail in [6] in 1D and defining $m_j^n = \min(c_{j-1}^n, c_j^n)$, $M_j^n = \max(c_{j-1}^n, c_j^n)$, we arrive at

$$\begin{cases} m_{j+1}^n \leq c_{j+\frac{1}{2}} \leq M_{j+1}^n, \quad \forall j \in \mathbb{Z}, \\ M_j^n + \frac{\Delta x}{u\Delta t}(c_j^n - M_j^n) \leq c_{j+\frac{1}{2}}^n \leq m_j^n + \frac{\Delta x}{u\Delta t}(c_j^n - m_j^n), \quad \forall j \in \mathbb{Z}, \\ |c_{j+1}^n - c_{j+\frac{1}{2}}^n| \text{ is minimum}, \quad \forall j \in \mathbb{Z}. \end{cases} \tag{16}$$

This minimization problem reduces to the explicit formula
first: compute some bounds

$$\begin{cases} b_j^n = \max(m_{j+1}^n, M_j^n + \frac{\Delta x}{u\Delta t}(c_j^n - M_j^n)), \\ B_j^n = \min(M_{j+1}^n, m_j^n + \frac{\Delta x}{u\Delta t}(c_j^n - m_j^n)). \end{cases}$$

then: compute the flux according to

$$c_{j+\frac{1}{2}}^n = \begin{cases} b_j^n \quad \text{if } c_{j+1}^n < b_j^n, \\ c_{j+1}^n \text{ if } b_j^n \leq c_{j+1}^n \leq B_j^n, \\ B_j^n \quad \text{if } B_j^n < c_{j+1}^n. \end{cases} \tag{17}$$

Of course an equivalent algorithm can be obtained in the case $u < 0$.

3.1 Properties of the scheme

We here just give an overview of the properties of this scheme. More details may be found in [18] and [6].

Lemma 1 The downwind limited scheme given in (16) or (17) is equivalent to the Ultra-Bee limiter ([25], [15], [24]), in the sense that

$$c^n_{j+\frac{1}{2}} = c^n_j + \max\left(0, \min((\frac{1}{\nu} - 1)r^n_j), 1\right)(c^n_{j+1} - c^n_j) \tag{18}$$

where $r^n_j = \frac{c^n_j - c^n_{j-1}}{c^n_{j+1} - c^n_j}$ is the ratio of slopes and $\nu = u\Delta t/\Delta x$.

The following result states that the downwind limited scheme is an exact scheme for a "dense" in L^1 set of functions.

Theorem 1 Let us assume that the discrete function $(c^n_j)_{j\in\mathbb{Z}}$ is such that $\exists \alpha \in [0, 1[$ such that $\forall j \in \mathbb{Z}$, $c^n_{3j+1} = c^n_{3j}$ and $c^n_{3j+2} = \alpha c^n_{3j+1} + (1-\alpha)c^n_{3j+3}$. Then

either $0 \leq \alpha + \nu < 1$**.** Let us set $0 \leq \bar{\alpha} = \alpha + \nu - 1 \leq 1$. Then for all j, $c^{n+1}_{3j+1} = c^{n+1}_{3j} = c^n_{3j}$ and $c^{n+1}_{3j+2} = (\bar{\alpha})c^{n+1}_{3j+1} + (1-\bar{\alpha})c^{n+1}_{3j+3}$.
or $1 \leq \alpha + \nu < 2$ Let us set $0 \leq \bar{\alpha} = \alpha + \nu - 1 \leq 1$. Then for all j $c^{n+1}_{3j+2} = c^{n+1}_{3j+1} = c_{3j+1}$ and $c^{n+1}_{3j+3} = (\bar{\alpha})c^{n+1}_{3j+2} + (1-\bar{\alpha})c^{n+1}_{3j+4}$.

The set of functions verifying hypothesis of theorem (1) is a set of step functions. In theorem 1, α is the same between each three points step. It is possible to replace three points step ($c_{3j+1} = c_{3j}$, $c_{3j+2} = \alpha c_{3j+1} + (1-\alpha)c_{3j+2}$), by four (or more) points steps with non-constant α ($c_{3j+2} = c_{3j+1} = c_{3j}$, $c_{3j+3} = \alpha_{3j+2}c_{3j+2} + (1-\alpha_{3j+2})c_{3j+4}$).

Since this scheme is exact for discontinuous functions and is convergent or all initial profiles (in particular for smooth initial profiles), then it is the algorithm we need for moving interfaces and mixing zones.

3.2 Numerical results

Let us now present some numerical results in order to give an overview of the capability of the scheme. First we focus on the 1D case. These test cases have been computed with periodic boundary conditions so that it is possible to be able to observe the result at a very long time.
Indicatrix function, figure 5: the first result is for an indicatrix function

in the interval $[0,1]$. The initial condition is $c_0(x) = 1$ if $0.4 \leq x \leq 0.6$ and $c_0(x) = 0$ otherwise. It illustrates the theorem (1) of exact advection. We see that this initial condition is not at all dissipated (figure 5, CFL number of 0.1)). Note that the result with the limited downwind scheme is exactly the projection of the continuous solution on the mesh. It is in this sense that we say that the limited downwind scheme is optimal for this kind of profiles.

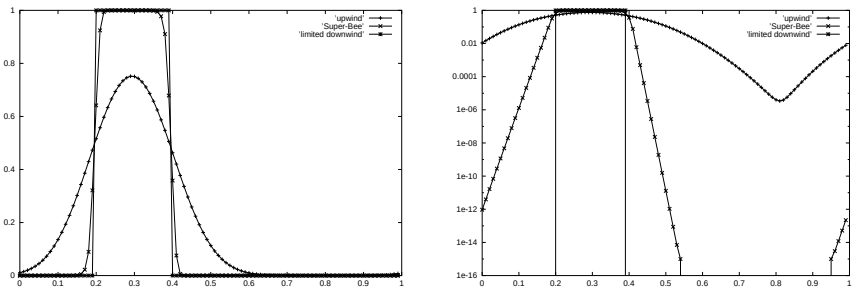

Fig. 5. Initial condition and results (limited downwind, Super-Bee limiter, upwind) for $t = 1$ (after one period). Log-scaled on the right. The initial condition (also exact solution) and the limited downwind result are confounded.

Academic mixing zone, figure 6: the initial condition is periodic and such that $c_0(x) = 1 - \frac{x}{0.3}$ if $x < 0.3$, $c_0(x) = 0$ if $0.3 \leq x < 0.7$ and $c_0(x) = \frac{x-0.7}{0.3}$ if $0.7 < x$. One sees that the upwind is highly dissipative, so that the numerical profile is a straight line for large times. On the contrary the Super-Bee scheme is subjected to the so-called overcompressivity pathology: the numerical profile is squared for large times. The important point is that the downwind scheme (also named Ultra-Bee scheme) is so overcompressive that local instantaneous overcompressivity takes place everywhere just after $t = 0$. The scheme is highly oscillating around smooth profiles, since this scheme is close to the linear downwind scheme. After this very linearly instable process, the scheme reaches its non-linear stability (TVD stability) and is exact.

Gaussian profile, figure 7: the initial condition is the Gaussian $c^0(x) =$

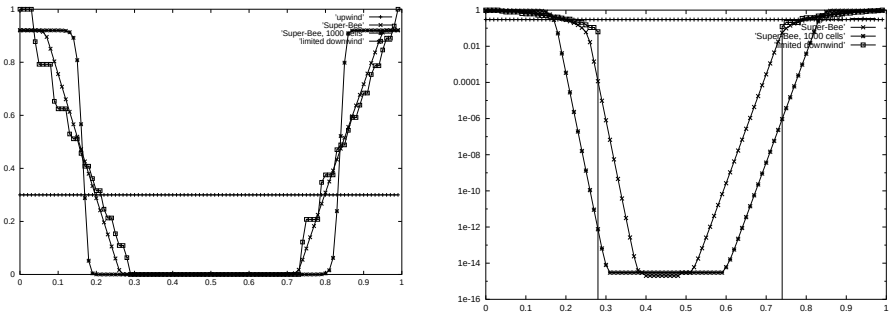

Fig. 6. Upwind, Super-Bee ($t = 100$), Super-Bee ($t = 1000$), limited downwind ($t = 100$, same result as $t = 1000$): 100 cells. Log-scaled on the right.

$e^{(-50x^2)}$, $\quad x \in [0,1]$. The numerical solution is also a Gaussian, except that

it has been transformed into a step Gaussian in a few time steps, and after has been exactly computed (we propose a zoomed view of the result in figure 7). Here, the result is given after 1000 periods, it is only indicative, the result being the same after any number of periods. It can be here compared to the result given by the Super-Bee scheme, showing its global over-compressive property. As expected, the results given by the upwind scheme are extremely diffused. As for the Gaussian test, the downwind scheme has transformed the initial condition into a step function and it then transports it exactly: the results after 2 and 20 periods are rigorously the same. The results for 500 cells show that the mean width of the steps is a constant (between 3 and 5) number of cells with respect to the mesh size. And when $\Delta x \to 0$, so does the width of the steps. Of course there exists schemes that can give better results after 2 periods, but the essential property of the presented one is that the numerical solution after any number of periods is the same as after 1 period (it is a conjecture, see [6]).

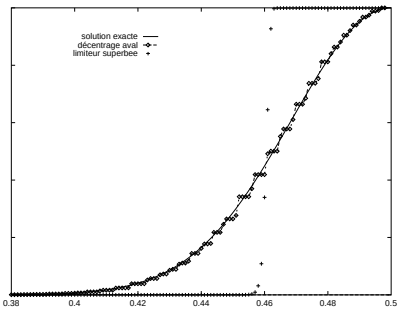

Fig. 7. Gaussian initial profile (exact solution, Super-Bee limiter and limited downwind scheme.)

We turn to the same problem in 2D $\partial_t c + u\partial_x c + v\partial_y c = 0$. We propose to use a very simple extension of what we have just presented: a dimensional splitting (the so-called Alternate Direction method) of the $2D$ equation in order to have only to solve $1D$ numerical problems. The principle is to solve alternatively the $1D$ equations $\partial_t c + u\partial_x c = 0$ and $\partial_t c + v\partial_y c = 0$. This method of course involves a Cartesian mesh. For each phase of the transport (x-phase and y-phase), we use the limited downwind scheme. We don't go further in details and just mention [18] where it is proved that this scheme is also exact for the transport of indicatrix functions, provided that these indicatrix functions may be geometrically decomposed in square indicatrix functions. We now present a few numerical results for the advection equation in dimension 2. The spatial domain we here consider is the square $[0,1[\times[0,1[\in \mathbb{R}^2$, again with periodic boundary conditions on $x = 0$, $x = 1$, $y = 0$ and $y = 1$. We choose as velocity the diagonal vector: $u = 1$, $v = 1$.

Indicatrix function in 2D, figure 3.2: the result reported on figures 3.2 for an indicatrix function is equivalent to that obtained for $1D$ advection: we have absolutely no dissipation for this test case. The numerical solution is **equal**

to the exact solution after one revolution. Once more it is in accordance with theoretical properties of the scheme, cf. [18]. This property of exact advection of square indicatrix functions has been proved for all directions $\vec{u} = (u, v) \in \mathbb{R}^2$ provided that $\frac{u}{v}$ is a rational number.

Gaussian profile in 2D, figures 9 and 10 However, the result obtained for the Gaussian initial function is not so satisfying because of the presence of oscillations. The limited downwind scheme with dimensional splitting is not TVD for the 2D definition of total variation, so oscillations may appear when computing regular solutions. It would be of interest to manage to add some constraints on the fluxes that would make the scheme TVD. A solution will be presented in section 5.

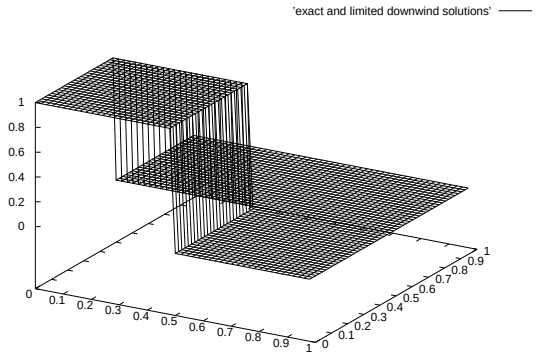

Fig. 8. Exact transport of a square: $t = 2$, $CFL = .25$

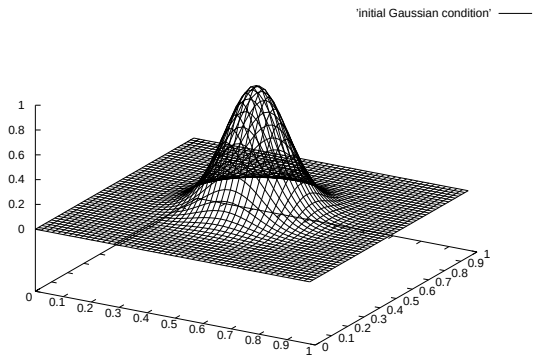

Fig. 9. The Gaussian profile: $t = 0$

4 The complete scheme

The complete scheme in $2D$ for the discretization of (9) simply consists in a double splitting: a Lagrange-projection splitting and a dimensional splitting.

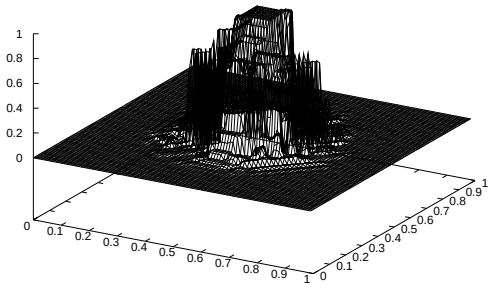

Fig. 10. The Gaussian profile: $t = 2$, $CFL = .25$

The dimensional splitting allows to deal with $1D$ problems only, which are based on a "Lagrange + projection" also called Lagrange + re-mapping decomposition of the system of partial differential equations: see for example [13] or [5]; but in the present work we propose to use a limited downwind scheme in the re-mapping stage of the algorithm instead of the classical upwind projection. As a simple example let us consider the $1D$ Euler system of compressible gas dynamics. Is is straightforward to prove that the left-hand side of (19) is, for smooth solutions, equivalent to the right-hand side

$$\begin{cases} \partial_t \rho + \partial_x(\rho u) = 0, \\ \partial_t \rho u + \partial_x(\rho u^2 + p) = 0, \\ \partial_t \rho ue + \partial_x(\rho ue + pu) = 0, \end{cases} \iff \begin{cases} \rho D_t \tau - \partial_x u = 0, \\ \rho D_t u + \partial_x p = 0, \\ \rho D_t e + \partial_x pu = 0, \end{cases} \tag{19}$$

where $D_t = \partial_t + u\partial_x$ is the convective derivative, and $\tau = 1/\rho$ is the specific volume. The numerical discretization of the right-hand side of (19) is the Lagrange part of the algorithm. Note that the Lagrange stage is a finite volume discretization of fluid dynamics in the comobile frame, that is in a reference frame which moves with the fluid. Then, of course, the re-mapping stage of the scheme is used to project the moving Lagrangian frame on the Cartesian fixed Eulerian frame. The key point of our algorithm is more in the re-mapping stage, where the computation the projection of the mass fractions uses a limited downwind procedure. In the following we only describe the x-part of the $2D$ algorithm.

4.1 The Lagrange computation

It corresponds to a finite volume numerical integration of the Lagrangian reformulation of (9) in the moving Lagrangian frame. We get, for the two

models presented in section 2

$$\begin{cases} \rho \mathrm{D}_t \tau - \partial_x u = 0, \\ \rho \mathrm{D}_t c_1 = 0, \\ \rho \mathrm{D}_t c_2 = 0, \\ \rho \mathrm{D}_t u + \partial_x p = 0, \\ \rho \mathrm{D}_t v = 0, \\ \rho \mathrm{D}_t e + \partial_x p u = 0, \\ p_1 = p_2 = p, \\ T_1 = T_2, \end{cases} \quad \text{or} \quad \begin{cases} \rho \mathrm{D}_t \tau - \partial_x u = 0, \\ \rho \mathrm{D}_t c_1 = 0, \\ \rho \mathrm{D}_t c_2 = 0, \\ \rho \mathrm{D}_t u + \partial_x p = 0, \\ \rho \mathrm{D}_t v = 0, \\ \rho \mathrm{D}_t e + \partial_x p u = 0, \\ p_1 = p_2 = p, \\ \mathrm{D}_t \varepsilon_1 + p_1 \mathrm{D}_t \tau_1 = \mathrm{D}_t \varepsilon_2 + p_2 \mathrm{D}_t \tau_2. \end{cases} \tag{20}$$

After discretization, one obtains for the x part of the Alternative Direction Splitting

$$\begin{cases} \rho_j \dfrac{\widetilde{\tau}_j - \tau_j}{\Delta t} - \dfrac{u_{j+1/2} - u_{j-1/2}}{\Delta x} = 0, \\ \rho_j \dfrac{\widetilde{u}_j - u_j}{\Delta t} + \dfrac{p_{j+1/2} - p_{j-1/2}}{\Delta x} = 0, \\ \widetilde{v}_j = v_j, \\ \rho_j \dfrac{\widetilde{e}_j - e_j}{\Delta t} + \dfrac{p_{j+1/2} u_{j+1/2} - p_{j-1/2} u_{j-1/2}}{\Delta x} = 0, \\ \widetilde{c}_j - c_j = 0, \qquad\qquad c = c_1 \text{ or } c_2, \end{cases} \tag{21}$$

with $\tau_j = 1/\rho_j$ for all cells (that is for all j). After this x finite volume discretization, one has to make a similar computation for the vertical y direction. As in [5], the fluxes in (21) are given by

$$\begin{cases} \rho c^*_{j+1/2} = \sqrt{\max(\rho_j {c_j}^2, \rho_{j+1} {c_{j+1}}^2) \min(\rho_j, \rho_{j+1})}, \\ p_{j+1/2} = \dfrac{p_j + p_{j+1}}{2} + \dfrac{\rho c^*_{j+1/2}}{2}(u_j - u_{j+1}), \\ u_{j+1/2} = \dfrac{1}{2\rho c^*_{j+1/2}}(p_j - p_{j+1}) + \dfrac{1}{2}(u_j + u_{j+1}), \end{cases}$$

together with $p_j = p(\rho_j, u_j, e_j)$ and $c_j = c(\rho_j, u_j, e_j)$. It remains to solve the mixture model. Since $(\widetilde{\tau}_j, \widetilde{u}_j, \widetilde{e}_j)$ have already been computed in (21), we first compute $\widetilde{\varepsilon}_j = e_j - \frac{1}{2}(\widetilde{u}_j)^2$, and then the following isobar-isothermal system composed of four equations: $c_1\widetilde{\tau}_{1j} + c_2\widetilde{\tau}_{2j} = \widetilde{\tau}_j$, $c_1\widetilde{\varepsilon_{1j}} + c_2\widetilde{\varepsilon_{2j}} = \widetilde{\varepsilon}_j$, $p_1(\widetilde{\tau}_{1j}, \widetilde{\varepsilon_{1j}}) = p_2(\widetilde{\tau}_{2j}, \widetilde{\varepsilon_{2j}})$ and $T_1(\widetilde{\tau}_{1j}, \widetilde{\varepsilon_{1j}}) = T_2(\widetilde{\tau}_{2j}, \widetilde{\varepsilon_{2j}})$. This is a system of four equations with four unknowns $(\widetilde{\tau}_{1j}, \widetilde{\tau}_{2j}, \widetilde{\varepsilon_{1j}}, \widetilde{\varepsilon_{2j}})$. It is possible to prove that this system has a unique solution provided both EOS is thermodynamically consistent. For perfect gas pressure laws, it is a exercise to get the exact solution (with

explicit formulae). Then one has to solve at each time step

$$\begin{cases} c_1\widetilde{\tau}_{1j} + c_2\widetilde{\tau}_{2j} = \widetilde{\tau}_j, \\ c_1\widetilde{\varepsilon}_{1j} + c_2\widetilde{\varepsilon}_{2j} = \widetilde{\varepsilon}_j, \\ p_1(\widetilde{\tau}_{1j}, \widetilde{\varepsilon}_{1j}) = p_2(\widetilde{\tau}_{2j}, \widetilde{\varepsilon}_{2j}), \\ \left[\varepsilon_{1j}\right] + p_1(\widetilde{\tau}_{1j}, \widetilde{\varepsilon}_{1j}) \left[\tau_{1j}\right] = \left[\varepsilon_{2j}\right] + p_2(\widetilde{\tau}_{2j}, \widetilde{\varepsilon}_{2j}) \left[\tau_{2j}\right] \end{cases} \tag{22}$$

where $[.]$ stands for $[f] = \widetilde{f} - f$. Here we have written the implicit discretization of the isobar-isoδQ closure, we let to the reader the explicit discretization, which has obviously the advantage of being cheaper from the computational point of view. However if one assumes perfect gas pressure law, then it is a simple exercise to get the exact analytical solution of (22). An interesting theoretical stability result will be stated in section 4.3 for the implicit system (22).

4.2 The advection part

This part of the scheme, also called projection or re-mapping, is a discrete approximation of $\partial_t\rho + u\partial_x\rho = 0$, $\partial_t c_1 + u\partial_x c_1 = 0$, $\partial_t c_2 + u\partial_x c_2 = 0$, $\partial_t u + u\partial_x u = 0$, $\partial_t v + u\partial_x v = 0$ and $\partial_t e + u\partial_x e = 0$, with either the isobar-isothermal closure ($p_1 = p_2 = p$, $T_1 = T_2$) or the isobar-isoδQ closure $p_1 = p_2 = p$ plus $\partial_t\varepsilon_1 + p\partial_t\tau_1 + u\partial_x\varepsilon_1 + pu\partial_x\tau_1 = \partial_t\varepsilon_2 + p\partial_t\tau_2 + u\partial_x\varepsilon_2 + pu\partial_x\tau_2$. This advection part can be understood as a numerical resolution of the convective derivative equation $\mathrm{D}_t U = 0$. The discretization of these systems is written in the classical following form, where the fluxes (which will be non-classical: limited downwind) will be precised later. Assume $u_{j+1/2} > 0 \quad \forall j \in \mathbb{Z}$, the x-part of the algorithm is

$$\begin{cases} \frac{\widehat{\rho}_j - \widetilde{\rho}_j}{\Delta t} + u_{j-1/2}\frac{\widetilde{\rho_{j+1/2}} - \widetilde{\rho_{j-1/2}}}{\Delta x} = 0, \\ \frac{\widehat{\rho}_j\widehat{c_{1,j}} - \widetilde{\rho}_j\widetilde{c_{1,j}}}{\Delta t} + u_{j-1/2}\frac{\widetilde{\rho_{j+1/2}}\widetilde{c_{1,j+1/2}} - \widetilde{\rho_{j-1/2}}\widetilde{c_{1,j-1/2}}}{\Delta x} = 0, \\ \frac{\widehat{\rho}_j\widehat{c_{2,j}} - \widetilde{\rho}_j\widetilde{c_{2,j}}}{\Delta t} + u_{j-1/2}\frac{\widetilde{\rho_{j+1/2}}\widetilde{c_{2,j+1/2}} - \widetilde{\rho_{j-1/2}}\widetilde{c_{2,j-1/2}}}{\Delta x} = 0, \\ \frac{\widehat{\rho}_j\widehat{u}_j - \widetilde{\rho}_j\widetilde{u}_j}{\Delta t} + u_{j-1/2}\frac{\widetilde{\rho_{j+1/2}}\widetilde{u_{j+1/2}} - \widetilde{\rho_{j-1/2}}\widetilde{u_{j-1/2}}}{\Delta x} = 0, \\ \frac{\widehat{\rho}_j\widehat{v}_j - \widetilde{\rho}_j\widetilde{v}_j}{\Delta t} + u_{j-1/2}\frac{\widetilde{\rho_{j+1/2}}\widetilde{v_{j+1/2}} - \widetilde{\rho_{j-1/2}}\widetilde{v_{j-1/2}}}{\Delta x} = 0, \\ \frac{\widehat{\rho}_j\widehat{e}_j - \widetilde{\rho}_j\widetilde{e}_j}{\Delta t} + u_{j-1/2}\frac{\widetilde{\rho_{j+1/2}}\widetilde{e_{j+1/2}} - \widetilde{\rho_{j-1/2}}\widetilde{e_{j-1/2}}}{\Delta x} = 0 \end{cases} \tag{23}$$

where of course $\widetilde{\rho_j} = 1/\widetilde{\tau}_j$. The discretization of the mixing model will be presented after. First notice that this discretization, combined with the Lagrange

part, gives

$$\left\{\begin{array}{c}
\frac{\widehat{\rho_j}-\rho_j}{\Delta t}+\frac{\widetilde{\rho_{j+1/2}}u_{j+1/2}-\widetilde{\rho_{j-1/2}}u_{j-1/2}}{\Delta x}=0,\\
\frac{\widehat{\rho_j}\widehat{c_{1,j}}-\rho_j c_{1,j}}{\Delta t}+\frac{\widetilde{\rho_{j+1/2}}\widetilde{c_{1,j+1/2}}u_{j+1/2}-\widetilde{\rho_{j-1/2}}\widetilde{c_{1,j-1/2}}u_{j-1/2}}{\Delta x}=0,\\
\frac{\widehat{\rho_j}\widehat{c_{2,j}}-\rho_j c_{2,j}}{\Delta t}+\frac{\widetilde{\rho_{j+1/2}}\widetilde{c_{2,j+1/2}}u_{j+1/2}-\widetilde{\rho_{j-1/2}}\widetilde{c_{2,j-1/2}}u_{j-1/2}}{\Delta x}=0,\\
\frac{\widehat{\rho_j}\widehat{u_j}-\rho_j u_j}{\Delta t}+\frac{\widetilde{\rho_{j+1/2}}\widetilde{u_{j+1/2}}u_{j+1/2}+p_{j+1/2}-\widetilde{\rho_{j-1/2}}\widetilde{u_{j-1/2}}u_{j-1/2}-p_{j-1/2}}{\Delta x}=0,\\
\frac{\widehat{\rho_j}\widehat{v_j}-\rho_j v_j}{\Delta t}+\frac{\widetilde{\rho_{j+1/2}}\widetilde{v_{j+1/2}}u_{j+1/2}-\widetilde{\rho_{j-1/2}}\widetilde{v_{j-1/2}}u_{j-1/2}}{\Delta x}=0,\\
\frac{\widehat{\rho_j}\widehat{e_j}-\rho_j e_j}{\Delta t}+\frac{\widetilde{\rho_{j+1/2}}\widetilde{e_{j+1/2}}u_{j+1/2}+p_{j+1/2}u_{j+1/2}-\widetilde{\rho_{j-1/2}}\widetilde{e_{j-1/2}}-p_{j-1/2}u_{j-1/2}}{\Delta x}=0,
\end{array}\right.$$

which shows that the global algorithm is consistent with Euler equations and conservative for all the natural conservative variables, *even for the mass of each component*. The other properties we want to ensure for the scheme are: positivity of mass fractions; entropy properties (positivity of the scheme); no dissipation on mass fractions in order to keep sharp interfaces and bounded mixing zones. The originality of the scheme presented here relies essentially on the fluxes chosen for the mass fractions c_1 and c_2: we use for it the limited downwind scheme (section 3); the resolution of the other equations is based on an upwind discretization. We first present the fluxes for the thermodynamic variables (fluxes which depend on the fluxes for c_1 and c_2) and in a second step give the anti-dissipative fluxes for mass fractions.

As just explained, the expression of the fluxes for the global thermodynamic variables (ρ, u, v, e) requires the knowledge of the fluxes $c_{1j+1/2}$ and $c_{2j+1/2}$. It requires too fluxes of thermodynamic quantities of each component: $\widetilde{\tau_{1,j+1/2}}$, $\widetilde{\tau_{2,j+1/2}}$, $\widetilde{\varepsilon_{1,j+1/2}}$, $\widetilde{\varepsilon_{2,j+1/2}}$. We simply take for these variables an upwind discretization:

- if $u_{j+1/2}\geq 0$: $\widetilde{\tau_{1,j+1/2}}=\widetilde{\tau_{1,j}}$, $\widetilde{\tau_{2,j+1/2}}=\widetilde{\tau_{2,j}}$, $\widetilde{\varepsilon_{1,j+1/2}}=\widetilde{\varepsilon_{1,j}}$ and $\widetilde{\varepsilon_{2,j+1/2}}=\widetilde{\varepsilon_{2,j}}$.
- if $u_{j+1/2}<0$: $\widetilde{\tau_{1,j+1/2}}=\widetilde{\tau_{1,j+1}}$, $\widetilde{\tau_{2,j+1/2}}=\widetilde{\tau_{2,j+1}}$, $\widetilde{\varepsilon_{1,j+1/2}}=\widetilde{\varepsilon_{1,j+1}}$ and $\widetilde{\varepsilon_{2,j+1/2}}=\widetilde{\varepsilon_{2,j+1}}$.

We now can define fluxes for the global thermodynamic variables as follows: $\widetilde{f_{j+1/2}}=\widetilde{c_{1,j+1/2}}\widetilde{f_{1,j+1/2}}+\widetilde{c_{2,j+1/2}}\widetilde{f_{2,j+1/2}}$, for $f=\tau$ or ε. The flux for the velocity variable is also up-winded. This gives explicitly (24-25)

$$\textbf{if } u_{j+1/2}\geq 0\left\{\begin{array}{l}
\widetilde{\rho_{j+1/2}}=\dfrac{1}{\widetilde{\tau_{j+1/2}}}=\dfrac{1}{\widetilde{c_{1,j+1/2}}\widetilde{\tau_{1,j}}+\widetilde{c_{2,j+1/2}}\widetilde{\tau_{2,j}}},\\
\widetilde{u_{j+1/2}}=\widetilde{u_j},\\
\widetilde{e_{j+1/2}}=\widetilde{c_{1,j+1/2}}\widetilde{\varepsilon_{1,j}}+\widetilde{c_{2,j+1/2}}\widetilde{\varepsilon_{2,j}}+\dfrac{1}{2}(\widetilde{u_j}^2+\widetilde{v_j}^2);
\end{array}\right. \tag{24}$$

$$\textbf{if } u_{j+1/2}<0 \begin{cases} \widetilde{\rho_{j+1/2}} = \dfrac{1}{\widetilde{\tau_{j+1/2}}} = \dfrac{1}{\widetilde{c_{1,j+1/2}\tau_{1,j+1}} + \widetilde{c_{2,j+1/2}\tau_{2,j+1}}}, \\ \widetilde{u_{j+1/2}} = \widetilde{u_{j+1}}, \\ \widetilde{e_{j+1/2}} = \widetilde{c_{1,j+1/2}\varepsilon_{1,j+1}} + \widetilde{c_{2,j+1/2}\varepsilon_{2,j+1}} + \dfrac{1}{2}(\widetilde{u_{j+1}}^2 + \widetilde{v_{j+1}}^2). \end{cases} \tag{25}$$

Equations (24) and (25) can be understood from a physical point of view: the fluxes of the exact solution verify these equation, that is why we ask the numerical solution to verify it. From a mathematical point of view, we will see in the following that this definition of the fluxes allows to get numerical entropy inequalities and are clearly consistent with (3) and (4). We now give the numerical mixture closures for the isobar-isothermal and for the isobar-isoδQ models. For the isobar-isothermal model we get $\widehat{c_{1,j}}\widehat{\tau_{1,j}}+\widehat{c_{2,j}}\widehat{\tau_{2,j}} = \widehat{\tau_j}$, $\widehat{c_{1,j}}\widehat{\varepsilon_{1,j}}+\widehat{c_{2,j}}\widehat{\varepsilon_{2,j}} = \widehat{\varepsilon_j}$, $p_1(\widehat{\tau_{1,j}},\widehat{\varepsilon_{1,j}}) = p_2(\widehat{\tau_{2,j}},\widehat{\varepsilon_{2,j}})$ and $T_1(\widehat{\tau_{1,j}},\widehat{\varepsilon_{1,j}}) = T_2(\widehat{\tau_{2,j}},\widehat{\varepsilon_{2,j}})$. As in the Lagrange part, it can be shown that this system of four equations with four unknowns $(\widehat{\tau_{1,j}},\widehat{\tau_{2,j}},\widehat{\varepsilon_{1,j}},\widehat{\varepsilon_{2,j}})$ has a solution under thermodynamic hypothesis. In the case of 2 ideal gas, it is easy to get the explicit analytical expression of the solution. For the isobar-isoδQ model we get the discrete system (26). where $[f] = \widehat{f} - \widetilde{f}$. The right-hand side term in last equation above in an approximation of $\Delta t(\rho u\partial_x(\varepsilon_2-\varepsilon_1) + \rho up\partial_x(\tau_2-\tau_1))$. This last equation is therefore consistent with $\rho\partial_t(\varepsilon_1-\varepsilon_2)+\rho p\partial_t(\tau_1-\tau_2)+\rho u\partial_x(\varepsilon_1-\varepsilon_2)+\rho up\partial_x(\tau_1-\tau_2) = 0$. Once more, it can be shown that in the case of two perfect gases, this system can be solved explicitly. We have already written it, the isobar-isoδQ model has the advantage of being numerically entropy-consistent through the consistent discretization (26).

$$\begin{cases} \widehat{c_{1,j}}\widehat{\tau_{1,j}} + \widehat{c_{2,j}}\widehat{\tau_{2,j}} = \widehat{\tau_j}, \\ \widehat{c_{1,j}}\widehat{\varepsilon_{1,j}} + \widehat{c_{2,j}}\widehat{\varepsilon_{2,j}} = \widehat{\varepsilon_j}, \\ p_1(\varepsilon_{1,j},\tau_{1,j}) = p_2(\varepsilon_{2,j},\tau_{2,j}) = \widehat{p_j}, \\ \widehat{\rho_j}([\varepsilon_{1,j}] + \widehat{p_j}[\tau_{1,j}] - [\varepsilon_{2,j}] - \widehat{p_j}[\tau_{2,j}]) \\ \quad = \lambda(u_{j+1/2}\widetilde{\rho_{j+1/2}}(\dfrac{\widetilde{c_{1,j+1/2}}}{\widehat{c_{1,j}}}((\widetilde{\varepsilon_{1,j}} - \widetilde{\varepsilon_{1,j+1/2}}) + \widehat{p_j}(\widetilde{\tau_{1,j}} - \widetilde{\tau_{1,j+1/2}})) \\ \qquad\qquad - \dfrac{\widetilde{c_{2,j+1/2}}}{\widehat{c_{2,j}}}((\widetilde{\varepsilon_{2,j}} - \widetilde{\varepsilon_{2,j+1/2}}) + \widehat{p_j}(\widetilde{\tau_{2,j}} - \widetilde{\tau_{2,j+1/2}}))) \\ \qquad - u_{j-1/2}\widetilde{\rho_{j-1/2}}(\dfrac{\widetilde{c_{1,j-1/2}}}{\widehat{c_{1,j}}}((\widetilde{\varepsilon_{1,j}} - \widetilde{\varepsilon_{1,j-1/2}}) + \widehat{p_j}(\widetilde{\tau_{1,j}} - \widetilde{\tau_{1,j-1/2}})) \\ \qquad\quad - \dfrac{\widetilde{c_{2,j-1/2}}}{\widehat{c_{2,j}}}((\widetilde{\varepsilon_{2,j}} - \widetilde{\varepsilon_{2,j-1/2}}) + \widehat{p_j}(\widetilde{\tau_{2,j}} - \widetilde{\tau_{2,j-1/2}})))). \end{cases} \tag{26}$$

All the algorithm for the projection part relies on the definition of the fluxes for mass fractions, and it is time now to describe these fluxes. We need some

fluxes $\widetilde{c_{1,j+1/2}}$ and $\widetilde{c_{2,j+1/2}}$ for the numerical mass conservation equations

$$\begin{cases} \widehat{\rho_j}\widehat{c_{1,j}} = \rho_j\widetilde{c_{1,j}} - \lambda(u_{j+1/2}\widetilde{\rho_{j+1/2}}\widetilde{c_{1,j+1/2}} - u_{j-1/2}\widetilde{\rho_{j-1/2}}\widetilde{c_{1,j-1/2}}), \\ \widehat{\rho_j}\widehat{c_{2,j}} = \rho_j\widetilde{c_{2,j}} - \lambda(u_{j+1/2}\widetilde{\rho_{j+1/2}}\widetilde{c_{2,j+1/2}} - u_{j-1/2}\widetilde{\rho_{j-1/2}}\widetilde{c_{2,j-1/2}}), \end{cases}$$

with

$$\begin{cases} \widehat{\rho_j} = \rho_j - \lambda(u_{j+1/2}\widetilde{\rho_{j+1/2}} - u_{j-1/2}\widetilde{\rho_{j-1/2}}), \\ \widetilde{\rho_{j+1/2}} = \dfrac{1}{\widetilde{c_{1,j+1/2}}\widetilde{\tau_{1,j}} + \widetilde{c_{2,j+1/2}}\widetilde{\tau_{2,j}}} \text{ if } u_{j+1/2} \geq 0, \\ \widetilde{\rho_{j+1/2}} = \dfrac{1}{\widetilde{c_{1,j+1/2}}\widetilde{\tau_{1,j+1}} + \widetilde{c_{2,j+1/2}}\widetilde{\tau_{2,j+1}}} \text{ if } u_{j+1/2} < 0. \end{cases}$$

The choice we do is to use limited downwind fluxes as presented in section 3 for the advection equation. This leads once more to an L^∞-stable, TVD and non-dissipative scheme. A complete presentation of this scheme together with some analysis of its properties can be found in [18], and a short explanation of the algorithm is reported in annex A.

4.3 Entropy properties

We now present the major properties of the scheme with the isobar-isoδQ model. We state two numerical entropy inequalities for the scheme used for the isobar-isoδQ model: one for the Lagrange part and one for the projection part. We refer to [4] for a complete and quite lengthy proof of these results.

Proposition 1 Entropy property in the Lagrange part Let us consider the Lagrangian scheme (21-22). Let $S_1(\varepsilon_1, \tau_1)$ and $S_2(\varepsilon_2, \tau_2)$ be concave entropies for fluids 1 and 2. Then there exist $c \in \mathbb{R}$ such that under the CFL condition $c\Delta t/\Delta x \leq 1$,

$$S_1(\widetilde{\varepsilon_{1,j}}, \widetilde{\tau_{1,j}}) \geq S_1(\varepsilon_{1,j}, \tau_{1,j}) \text{ and } S_2(\widetilde{\varepsilon_{2,j}}, \widetilde{\tau_{2,j}}) \geq S_2(\varepsilon_{2,j}, \tau_{2,j}) \quad \forall j \in \mathbb{Z}. \quad (27)$$

The number c is an approximate value of the maximum of the (mixture) sound speed in all the cells. Inequality (27) simply explains that the scheme is entropy consistent in the Lagrange part. The following proposition 2 now states an entropy result for the scheme independent on the mass fraction fluxes $\widetilde{c_{1,j+1/2}}$, $\widetilde{c_{2,j+1/2}}$.

Proposition 2 Entropy property in the re-mapping part Assume that some very natural conditions are verified: positivity of temperatures, mass fractions, densities. The positivity of temperature is simply $T_1(\widehat{\varepsilon_{1,j}}, \widehat{\tau_{1,j}}) > 0$ and $T_2(\widehat{\varepsilon_{2,j}}, \widehat{\tau_{2,j}}) > 0$. We refer to [18] for the precise statement of all other positive inequalities. Then we obtain entropy inequalities for all entropies in

the re-mapping part of the algorithm, in the sense that for every $j \in \mathbb{Z}$ ($r = 1, 2$)

$$S_r(\widehat{\varepsilon_{r,j}}, \widehat{\tau_{r,j}}) \geq \min\left(S_r(\widetilde{\varepsilon_{r,j}}, \widetilde{\tau_{r,j}}), S_r(\widetilde{\varepsilon_{r,j-1}}, \widetilde{\tau_{r,j-1}}), S_r(\widetilde{\varepsilon_{r,j+1}}, \widetilde{\tau_{r,j+1}})\right).$$

This proves that the entropy in each cell after the projection part is greater than the entropy before. A more precise statement of this property is in [18]. A very remarkable feature of these inequalities is that there are true whatever the fluxes of the mass fractions are, the only requirement being that all other fluxes are compatible with the fluxes of the mass fractions (24-25). So it explains that the thermodynamic stability of the scheme is independent on the scheme used for the mass fractions and justify the use of a highly anti-dissipative down-winded scheme for the mass fractions in conjunction with an up-winded scheme for all thermodynamic variables.

5 Numerical results

We study hydrodynamic instabilities, the first one is the Kelvin-Helmholtz instability, the second one the Richtmyer-Meshkov instability. Then we study the interaction of shock with a mixing zone. It clearly reveals the interest of a mixed limited downwind-order two scheme. Many 1D results can be founded in [18]: here we restrict the presentation to a simple model with dynamic mixing.

5.1 Hydrodynamic instabilities in 2D

5.1.1 A Kelvin-Helmholtz instability

The Kelvin-Helmholtz instability is a shear layer hydrodynamic instability. Here the equation of the initial interface between the 2 fluids is $y = f(x) = 0,025\sin(2\pi x)$. This interface is a contact discontinuity where the tangential part of the velocity is discontinuous. On the boundaries $x = 0$ and $x = 1$, we impose periodic conditions (simulating an infinite sinusoid) and some wall-condition on $y = 0$ and $y = 1$.

For $t > 0$ the interface winds and becomes a kind of spiral. The result in figure 11 has been computed with 300×300 cells, for time 6.1. We can compare solutions computed with the classical upwind scheme and the limited downwind scheme (both used for the projection of mass fractions). We observe that the scheme with limited downwind fluxes for the mass fractions does not introduce any spreading of the interface. Note that iso-lines 0.999 and 0.001 are almost equal on the numerical result, which shows the accuracy of the

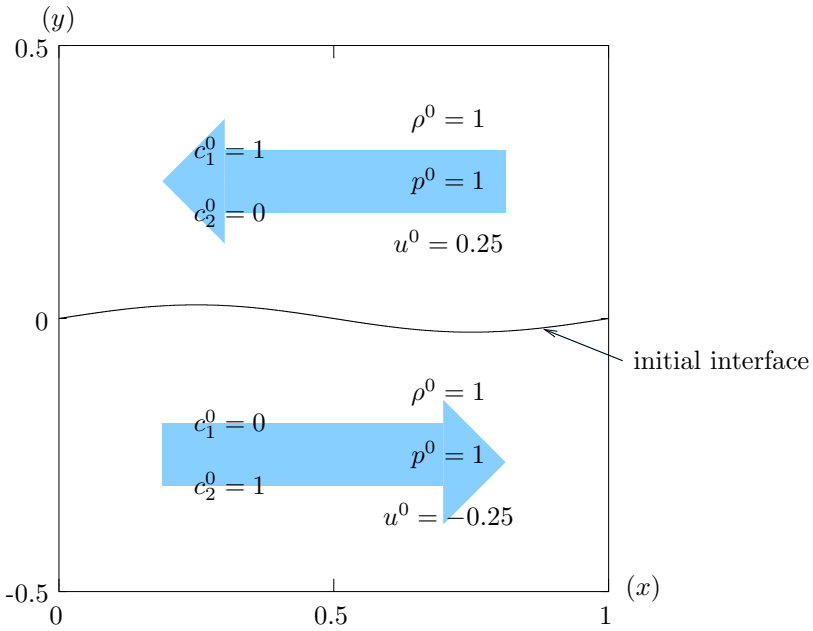

algorithm near interfaces. This allows to follow with an increased accuracy the interfacial instability. The presence of steps along the interface is a small drawback in this case. This result is comparable to those obtained with front tracking methods.

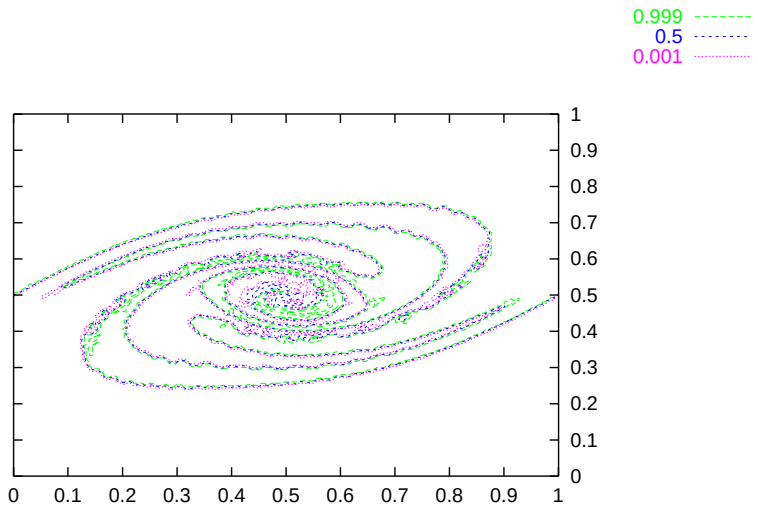

Fig. 11. Iso-lines of the Kelvin-Helmholtz instability, 90 000 cells.

5.1.2 A Richtmyer-Meshkov instability

This instability appears when a shock impinges an interface between 2 components, coming from the light fluid and going into the heavy fluid. We here choose initial conditions of the test-case proposed by [11] (this is the so called "Stony Brook" test case). The interface equation is $y = f(x) =$

$0.005\cos(2\pi x/0,036) + 0.12$. Initial values are

$$\begin{cases} y > f(x) & c_1 = 1\ c_2 = 0\ \rho = 2.95\ p = 50000 \quad u = 0\ v = -453, \\ 0.09 < y < f(x) & c_1 = 0\ c_2 = 1\ \rho = 1.87\ p = 50000 \quad u = 0\ v = -453, \\ y < 0.09 & c_1 = 0\ c_2 = 1\ \rho = 6.01\ p = 753000\ u = 0\ v = 55.5. \end{cases}$$

Since the discontinuity at $y = 0.09$ is a pure shock, then the solution is such that a pure shock arrives on the interface. After this, a typical "mushroom" instability is observed: this is the Richtmyer-Meshkov instability. Let us observe on figure 12 the mass fraction c_1 at $t = 0.00105$, computed with the scheme proposed in this work. The sharpness of the interface is almost perfect, since all iso-lines $0.001 \leq c_1 \leq 0.999$ are graphically the same.

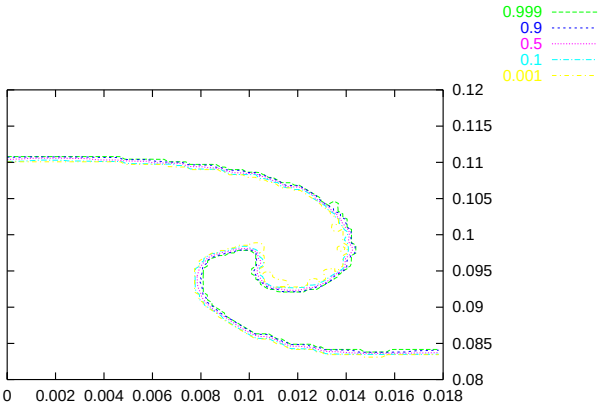

Fig. 12. Iso-lines of the Richtmyer-Meshkov instability, 60× 334 cells.

5.2 Mixing zones in 2D

Next we study the interaction of a shock with a mixing zone. Numerical results are given in figure 13. The initial condition are those of a convergent Sod shock tube, that is, $\rho = p = 1$, $u = v = 0$ for $\sqrt{x^2 + y^2} > 0.5$, $\rho = 0.125$, $p = 0.1$, $u = v = 0$ for $\sqrt{x^2 + y^2} < 0.5$, $c_1 = 0$ for $\sqrt{x^2 + y^2} > 0.8$ and $c_1 = 1$ for $\sqrt{x^2 + y^2} > 0.2$. The mass fraction c_1 is affine in $\sqrt{x^2 + y^2}$ for $0.2 \leq \sqrt{x^2 + y^2} \leq 0.8$. In this simulation, the mixing zone exists at $t = 0$: this is what we call **static mixing**. For small times, the numerical solution is a convergent shock. After the rebound of the shock the value of the mass fraction is given in figure 13. Note that the edges of the mixing zone are perfect, in the sense that almost zero spreading of the edges is added by the scheme. However we note some oscillations in the middle of the mixing zone (recall oscillations for the 2D Gaussian in the case of advection). Note however that these oscillations do not enter in contradiction with the entropy inequalities

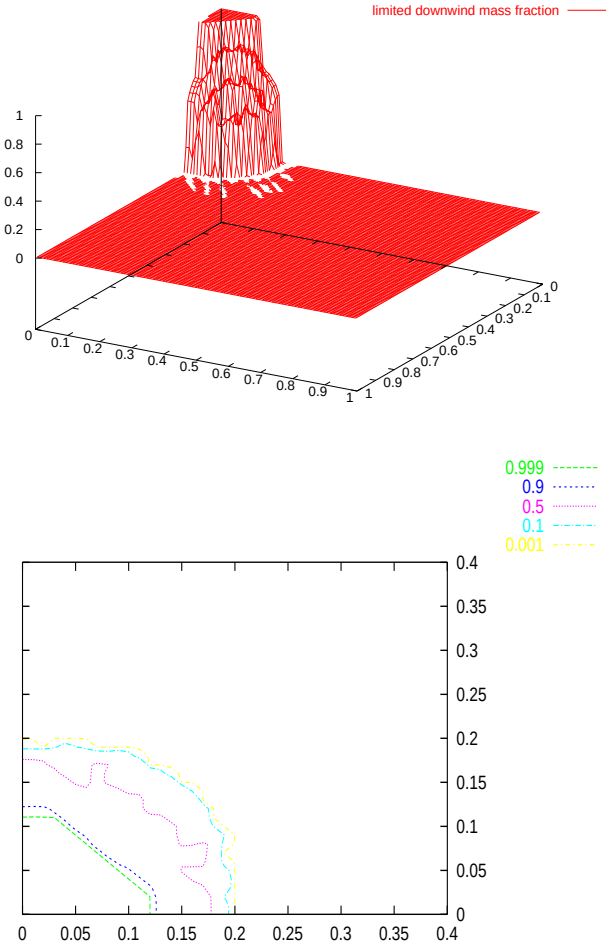

Fig. 13. Shock-mixing zone interaction. From top to bottom: mass fraction and iso-lines of the mass fraction.

of propositions 1 and 2, since the entropy is a thermodynamic variable which does not depend on c_1 and c_2. On the contrary the oscillations are clearly bounded in L^∞ but are not bounded in the BV norm for c_1 and c_2. This was already explained in section 3.2 for the Gaussian profile in 2D. So it reveals the need for a non-oscillating algorithm in the mixing zone, coupled with the anti-diffusive algorithm on the edge of this mixing zone. In figures 14 and 15, we have precisely used such a coupled algorithm. The best results are obtained with a MUSCL-type second order limiter [13], [25] in the mixing zone, coupled with our algorithm in the edges of the mixing zone. At each cell we check if the mass fraction is between two values c_- and c_+ with $0 < c_- < c_+ < 1$. We apply the second order MUSCL type limiter for $c_- < c < c_+$, and our anti-dissipative algorithm for $c \geq c^+$ and $c \leq c^-$. The value used in following computations is $c_- = 0.005 = 1 - c_+$. By inspection of the numerical results, we note that the anti-dissipative algorithm is oscillating in the mixing zone (as this was shown in figure 13), that the MUSCL type limiter used everywhere (i.e. for $0 \leq c \leq 1$) gives a smooth profile in the mixing zone but at the

price of a huge spreading of the edges of the mixing zone (see figure 15). The coupled algorithm gives here very good results, with the accuracy of the anti-dissipative algorithm on the edges and the smoothness of a more classical scheme inside the mixing zone. A zoom on the edges is given in figure 15, identical to figure 14 but log-scaled.

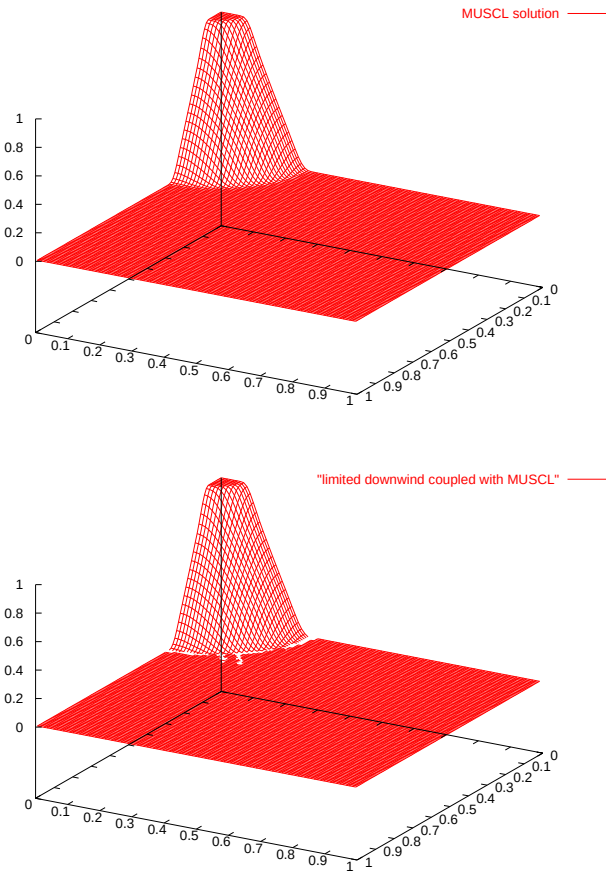

Fig. 14. After focalization and rebound of the shock. From top to bottom: a second order MUSCL-type approach; a second order MUSCL-type approach coupled with downwind limited on the edges. Results must be compared with figure 13.

6 Dynamic mixing

This section is devoted to present a very simple extension of the model and the algorithm to **dynamic mixing**. We add a Fick diffusion right-hand side in (9) in order to model the transition from an interface at $t = 0$ to a mixing zone with compact support. In contrary to the results of section 5, there is no mixing zone at $t = 0$, but there is one for some time $T > 0$, which is characteristic of dynamic mixing. The model we study is an extension of the

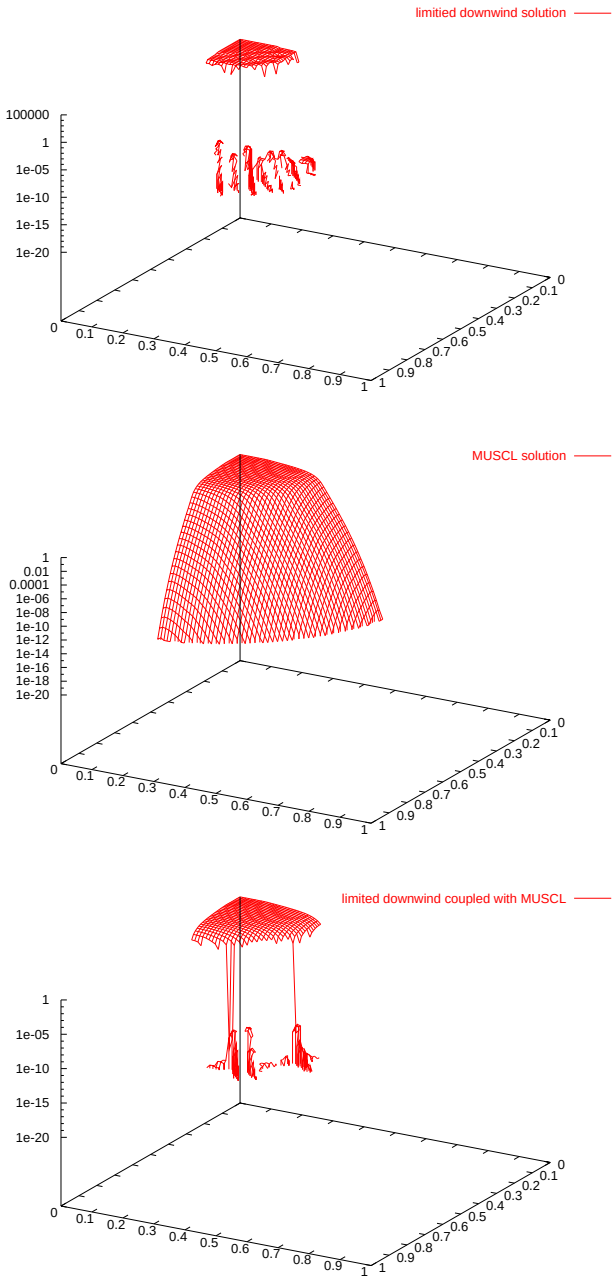

Fig. 15. The mass fraction, log-scaled. From top to bottom: downwind limited scheme; a second order MUSCL type approach; a second order MUSCL type approach coupled with downwind limited on the edges.

isobar-isothermal 1D model

$$\begin{cases} \partial_t \rho + \partial_x(\rho u) = 0, \\ \partial_t(\rho c_1) + \partial_x(\rho u c_1) = \partial_x(K \partial_x c_1), \\ \partial_t(\rho c_2) + \partial_x(\rho u c_2) = \partial_x(K \partial_x c_2), \\ \partial_t(\rho u) + \partial_x(\rho u^2 + p) = 0, \\ \partial_t(\rho e) + \partial_x(\rho u e + p u) = 0, \\ p_1 = p_2 = p, \\ T_1 = T_2. \end{cases} \tag{28}$$

where the diffusion coefficient is a non linear functional with respect to the mass fraction $K = a(c_1c_2)^m$ ($a > 0$ and $m > 0$). Numerical results for a simple experiment are given in figures 17 to 20. The initial condition are given in figure 16. The numerical results were obtained with a splitting strategy: first we solve the homogeneous hyperbolic left-hand side of system (28), second we solve a implicit discretization of the non linear diffusion equation with an explicit value of the diffusion coefficient.

Let us describe a little the results: $a = 0.25$, $m = 2$, $CFL = 0.6$. At $t = 0$, figure 16, the interface is at $x = 0.5$. Then a shock comes on the interface. As long as the shock does not interact with the interface, the numerical value of the diffusion is $K = a(c_1c_2)^m = 0$ in the neighborhood of the interface. Thus the diffusion operator does not play any role in the simulation: indeed until figure 18, we see that the problem reduces to a pure hydrodynamic computation. But in figure 18 the shock is on the interface. Now due to the fact that the velocity is non-zero after the shock, both mass fractions c_1 and c_2 are transported on the mesh. So these mass fractions take intermediate values in at least one cell. In these cells one has $c_1c_2 > 0$ so the coefficient in the diffusion operator is positive: it leads to non linear diffusion effect which is, in this simulation, the cause of the dynamic mixing. This is illustrated in figures 19 and 20. This scenario is typical of a dynamical mixing. Note however that this kind of numerical results are heavily dependent on some mathematical properties of the non-linear degenerate diffusion operator which is on the right-hand side of (28). It is indeed the fact that the same Cauchy problem for some given non linear degenerate diffusion heat equation has two different solutions which render possible this kind of modeling of dynamic mixing. More theoretical studies are needed. The simulations are only here to illustrate the capabilities of the algorithm.

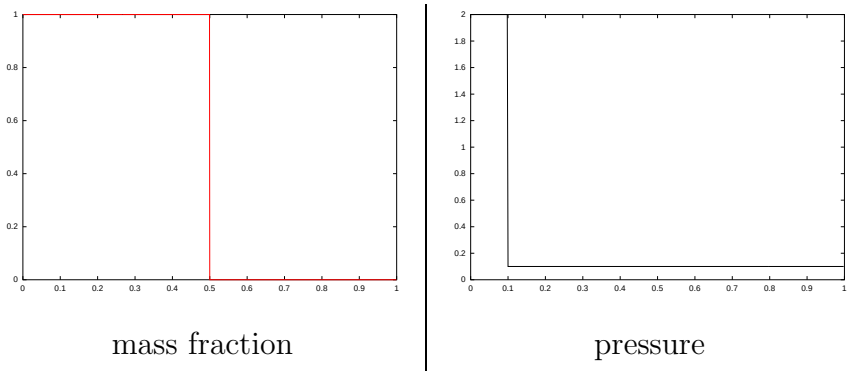

Fig. 16. Mass fraction and pressure, $t = 0$.

Acknowledgements This research was done when both authors were at the Commissariat à l'Énergie Atomique, France. Both authors are greatly indebted to H. Jourdren (CEA) for his presentation of multi-component compressible fluid dynamics simulation and thank

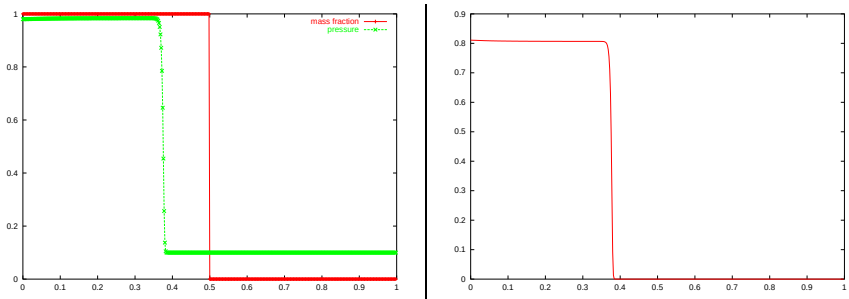

mass fraction and pressure | velocity

Fig. 17. $t = 0.25$: the interface ($x = 0.5$) is still ahead of the shock ($x \approx 0.4$).

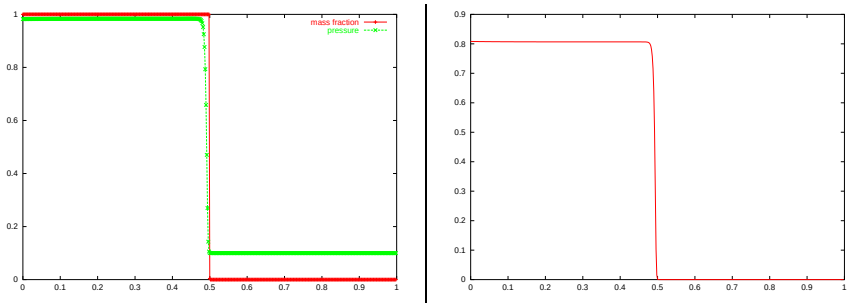

mass fraction and pressure | velocity

Fig. 18. $t = 0.356$: the shock is on the interface $x = 0.5$.

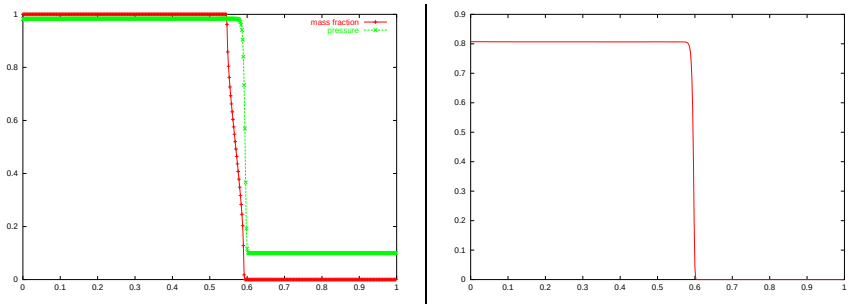

mass fraction and pressure | velocity

Fig. 19. $t = 0.45$: the shock has passed through the interface.

A. Davroux for the numerical simulations of the coupled algorithm for mixing zones, and L. Pierrejean for the numerical study of the dynamical mixing zone.

References

[1] R. Abgrall, Généralisation du schéma de Roe pour le calcul d'écoulements de mélanges de gaz à concentrations variables, La recherche aérospatiale, 1989.

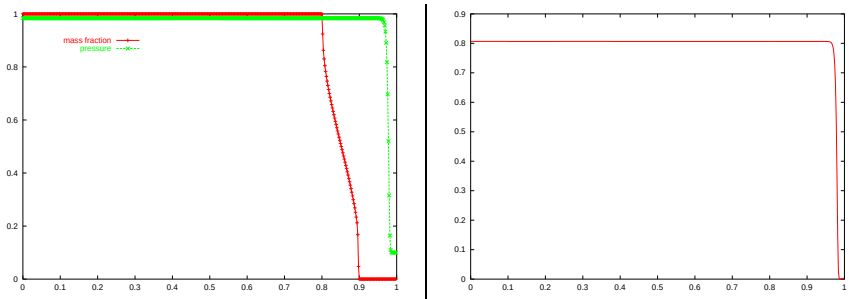

mass fraction and pressure | velocity

Fig. 20. $t = 0.8$: the shock is now away from the mixing zone which has been dynamically created by the shock.

[2] D. Chargy, R. Abgrall, L. Fezoui and B. Larrouturou, Comparisons of several upwind schemes for multi-component one-dimensional inviscid flows, INRIA, 1990.

[3] P. Colella, Volume-of-Fluid methods for partial differential equations, Godunov methods, published by E. Toro, Kluwer Academic/Plenum Publishers, 2001.

[4] B. Després, Construction, analyse et discrétisation d'un modèle de dynamique des fluides compressibles multi-constituants, Technical report CEA, 1997.

[5] B. Després, Inégalités entropiques pour un solveur de type Lagrange+projection des équations de l'hydrodynamique, Technical report CEA, 1997.

[6] B. Després and F. Lagoutière, Contact discontinuity capturing schemes for linear advection and compressible gas dynamics, to appear in JSC.

[7] B. Després and F. Lagoutière, Un schéma non linéaire anti-dissipatif pour l'équation d'advection linéaire, Comptes Rendus de l'Académie des Sciences, 1999.

[8] G. Allaire, S. Clerc and S. Kokh, A five-equation model for the numerical simulation of interfaces in two-phase flows, Comptes Rendus de l'Académie des Sciences, 2000.

[9] R.P. Fedkiw and T. Aslam and B. Merriman and S. Osher, A non-oscillatory eulerian approach to interfaces in multi-material flows (the ghost fluid method), Journal of Computational Physics, 152, 457–492, 1999.

[10] I.L. Chern, J. Glimm, O. McBryan, B. Plohr and S. Yaniv, Front tracking method for hyperbolic conservation laws, Journal of Computational Physics, 62, 83–110, 1986.

[11] Y Chen, J. Glimm, D. H. Sharp and Q. Zhang, A two-phase flow model of the Rayleigh-Taylor mixing zone, Report of the University of Stony Brook (1995).

[12] J. Glimm, J.W. Grove, X. L. Li, K-M. Shyue, Y. Zeng and Q. Zhang, Three dimensional front tracking, Report of the University of Stony Brook (1996).

[13] E. Godlewski and P.-A. Raviart, Numerical approximation of hyperbolic systems of conservation laws, Springer 1995.

[14] J.F. Hass, L. Schwaerdele, G. Jourdan and L. Houas, Hot wire measurements of the local Reynolds number in a turbulent mixing zone induced by the Richtmyer-Meshkov instability in a shock tube, in proceedings of the Second international Conference on Inertial Fusion and Apllications, (2001) Kyoto.

[15] H. Harten, On a class of high resolution total-variation-stable finite-difference schemes, SIAM Jour. of Numer. Anal., 21 (1), (1984) 1–23.

[16] H. Harten, High resolution schemes for hyperbolic conservation laws, J. Comp. Phys., 49, (1983) 357–393.

[17] C.W. Hirt and B.D. Nichols, Volume-of-fluid (VOF) method for the dynamics of free boundaries, J. Comp. Phys., 39, 201–225, 1981.

[18] F. Lagoutière, Modélisation mathématique et résolution numérique de problèmes de fluides compressibles à plusieurs constituants, PhD dissertation, University Paris-VI, 2000.

[19] X.D. Liu and R.P Fedkiw and S. Osher, A quasi-conservative approach to the multiphase Euler equations without spurious oscillations, Comp. And Applied Math., 11, UCLA, 1998.

[20] W. F. Noh and P. R. Woodward, SLIC (Simple line interface calculation), Springer Lecture Notes in Physics, 25:330–339, 1976.

[21] S. Osher and J.A. Sethian, Front propagating with curvature-dependent speed: algorithms based on Hamilton-Jacobi formulations, Journal of Computational Physics, 79, 12–49, 1988.

[22] R. Saurel and R. Abgrall, A simple method for compressible fluid flows, Journal of Computational Physics, 1997.

[23] R. Saurel and R. Abgrall, A multiphase Godunov method for compressible multifluid and multiphase flows, Journal of Computational Physics, 1999.

[24] P.K. Sweby, High resolution schemes using flux limiters for hyperbolic conservation laws, SIAM J. Num. Anal., 21, (1984), 995—1011.

[25] E. F. Toro, Riemann Solvers and Numerical Methods for Fluid Dynamics, (Springer-Verlag 1997).

[26] S.T. Zalesak, Fully multidimensional flux-corrected transport algorithms for fluids, Journal of Computational Physics, 31, 335–362,1979.

A Non-dissipative algorithm for the mass fractions

The method for deriving the present scheme is rigorously the same as reported in [6] for linear advection equation and for Euler equation. The principle is to

write some stability (L^∞ and TVD) constraints on the mass fractions c_1 and c_2 and to deduce from it some sufficient conditions on each mass fraction flux. Avoiding explaining the algorithm in detail (which is done in [18]), let us just briefly describe it.

We need the definition of the following quantities.

$$\begin{cases} \widetilde{s_{j+1/2}} = \lambda u_{j+1/2} + \rho_j(\widetilde{M_{j-1/2}} - \widetilde{c_{1,j}})(\widetilde{\tau_{1,j}} - \widetilde{\tau_{2,j}}), \\ \widetilde{t_{j+1/2}} = \rho_j(\widetilde{c_{1,j}} - \widetilde{M_{j-1/2}})\widetilde{\tau_{2,j}} + \widetilde{M_{j-1/2}}\lambda u_{j+1/2}, \\ \widetilde{v_{j+1/2}} = \lambda u_{j+1/2} + \rho_j(\widetilde{m_{j-1/2}} - \widetilde{c_{1,j}})(\widetilde{\tau_{1,j}} - \widetilde{\tau_{2,j}}), \\ \widetilde{w_{j+1/2}} = \rho_j(\widetilde{c_{1,j}} - \widetilde{m_{j-1/2}})\widetilde{\tau_{2,j}} + \widetilde{m_{j-1/2}}\lambda u_{j+1/2}, \end{cases}$$

In order the scheme (23) to be stable for mass fractions, it is sufficient to have

$$\widetilde{c_{1,j+1/2}}\widetilde{s_{j+1/2}} \geq \widetilde{t_{j+1/2}},\ \widetilde{c_{1,j+1/2}}\widetilde{v_{j+1/2}} \leq \widetilde{w_{j+1/2}},\ \widetilde{m_{j+1/2}} \leq \widetilde{c_{1,j+1/2}} \leq \widetilde{M_{j+1/2}}.$$

Thus explicit form of the fluxes $c_{1j+1/2}$ and $c_{2j+1/2}$ depends on the signs of $\widetilde{s_{j+1/2}}$ and $\widetilde{v_{j+1/2}}$. First remark that because of their definition, these two numbers cannot be simultaneously negative.

- If $\widetilde{s_{j+1/2}} > 0$ and $\widetilde{v_{j+1/2}} > 0$, we define $\widetilde{\gamma_{j+1/2}} = \max(\widetilde{t_{j+1/2}}/\widetilde{s_{j+1/2}}, \widetilde{m_{j+1/2}})$ and $\widetilde{\Gamma_{j+1/2}} = \min(\widetilde{w_{j+1/2}}/\widetilde{v_{j+1/2}}, \widetilde{M_{j+1/2}})$.
- if $\widetilde{s_{j+1/2}} > 0$ and $\widetilde{v_{j+1/2}} < 0$, we define $\widetilde{\gamma_{j+1/2}} = \max(\widetilde{t_{j+1/2}}/\widetilde{s_{j+1/2}}$, $\widetilde{w_{j+1/2}}/\widetilde{v_{j+1/2}}, \widetilde{m_{j+1/2}})$ and $\widetilde{\Gamma_{j+1/2}} = \widetilde{M_{j+1/2}}$.
- if $\widetilde{s_{j+1/2}} < 0$, $\widetilde{v_{j+1/2}} > 0$ and we define $\widetilde{\gamma_{j+1/2}} = \widetilde{m_{j+1/2}}$ and $\widetilde{\Gamma_{j+1/2}} = \min(\widetilde{t_{j+1/2}}/\widetilde{s_{j+1/2}}, \widetilde{w_{j+1/2}}/\widetilde{v_{j+1/2}}, \widetilde{M_{j+1/2}})$.
- if $\widetilde{s_{j+1/2}} = 0$ (resp. $\widetilde{v_{j+1/2}} = 0$), we define $\widetilde{\gamma_{j+1/2}} = \widetilde{m_{j+1/2}}$ and $\widetilde{\Gamma_{j+1/2}} = \widetilde{M_{j+1/2}}$.

Then the limited downwind flux is defined as

$$\begin{array}{l} \widetilde{c_{1,j+1/2}} = \widetilde{\gamma_{j+1/2}} \text{ if } \widetilde{c_{1,j+1}} \leq \widetilde{\gamma_{j+1/2}}, \\ \widetilde{c_{1,j+1/2}} = \widetilde{c_{1,j+1}} \text{ if } \widetilde{\gamma_{j+1/2}} \leq \widetilde{c_{1,j+1}} \leq \widetilde{\Gamma_{j+1/2}}, \\ \widetilde{c_{1,j+1/2}} = \widetilde{\Gamma_{j+1/2}} \text{ if } \widetilde{\Gamma_{j+1/2}} \leq \widetilde{c_{1,j+1}}. \end{array}$$